Check for updates

Impacts of model resolution on responses of western North Pacific tropical cyclones to ENSO in the HighResMIP-PRIMAVERA ensemble

Jingchan Liu, Chaoxia Yuan* and Jing-Jia Luo

Key Laboratory of Meteorological Disaster of Ministry of Education (KLME), Collaborative Innovation Center on Forecast and Evaluation of Meteorological Disasters, Institute for Climate and Application Research (ICAR), Nanjing University of Information Science and Technology, Nanjing, China

The El Niño/Southern Oscillation (ENSO) is the major driver of interannual variations of the western North Pacific (WNP) tropical cyclones (TCs). Realistic reproduction of ENSO-WNPTC teleconnection in coupled models (CGCMs) is thus crucial for improved seasonal-to-interannual prediction of WNPTC activity. Here, basing on the outputs of six pairs of high-resolution (HR) and low-resolution (LR) CGCMs participating the HighResMIP-PRIMAVERA project, we showed that the HR models outperform the LR ones in reproducing the observed increase of TC genesis in the southeastern WNP but the decrease in the northwestern WNP in the developing years of El Niño. The better performance of HR than LR models is on one hand due to the generally increased frequency and variability of TCs in the HR models. On the other hand, the teleconnection of El Niño to the WNP shows a dipole circulation difference between the HR and LR models with an anomalous cyclone in the southeastern WNP and anticyclone in the northwestern WNP, which enhances the dipole TC genesis anomalies in the HR compared to the LR models. The teleconnection difference stems from the westward shift of the ENSO-related SST and convection anomalies in the tropical Pacific in the HR compared to the LR models, which may be ultimately linked to the reduced cold tongue biases in the HR models.

KEYWORDS

ENSO, western North Pacific tropical cyclones, HighResMIP-PRIMAVERA, coupled model resolution, cold tongue bias

1 Introduction

The Western North Pacific (WNP) is the most active ocean basin of tropical cyclone (TC) activity; about one-third of global TCs are generated there (Elsberry, 2004; Zhang et al., 2016b; Gong et al., 2022). The TCs are highly destructive owing to the associated strong wind and heavy rain, and thus often cause huge losses in economic and ecosystem when landing. For example, super typhoon Lekima in 2019 impacted over 14 million people in China, and caused direct economic loss up to 53.72 billion Chinese Yuan (Zhang et al., 2009; Peduzzi et al., 2012; Zhao, 2019). Hence, improved understanding of TC activity is crucial for its better simulation, prediction and mitigation.

The El Niño-Southern Oscillation (ENSO) is the primary driver of interannual variations in the WNPTC activity including the TC genesis, track, lifetime, intensity and landfall by

modifying the regional sea surface temperatures (SSTs), vertical wind shear, relative vorticity, monsoonal trough and large-scale steering flow (Gray, 1979; Ritchie and Holland, 1999; Shay et al., 2000; Emanuel, 2005; Chih and Wu, 2020). In the developing year of El Niño, the genesis location of WNPTC shifts significantly southeastward, while the total number does not change much (Chan, 2000; Wang and Chan, 2002; Zhao and Wang, 2018). Meanwhile, the TCs become more intense and long-lived and tend to have northward recurving tracks. In contrast, in the developing year of La Niña, the genesis location of WNPTC shifts significantly northwestward, and the TCs are more likely to travel westward and make landfall in East Asia (Wang and Chan, 2002; Camargo and Sobel, 2005). Hence, realistic simulation of ENSO (i.e., Indo-western Pacific Ocean capacitor (IPOC) effect in the El Niño following summer) impacts on the WNPTCs is vital to accurate prediction of the WNPTC activity (Takaya et al., 2021), especially considering that the ENSO is the most predictable signal at the seasonal-to-interannual time scale in our climate system and provides the fundamental source of the TC predictability (Vecchi et al., 2014).

For decades, huge efforts have been made to reproduce the ENSO-WNPTC teleconnection in the numerical models (Wu and Lau, 1992; Camargo and Sobel, 2005; Iizuka and Matsuura, 2007; Murakami et al., 2011; Bell et al., 2014; Zhang et al., 2016a; Krishnamurthy et al., 2016). It seems that the shift of TC genesis location in the ENSO years can be well simulated by both the atmospheric general circulation models (AGCMs) and the coupled general circulation models (CGCMs) (Wu and Lau, 1992; Murakami et al., 2011; Krishnamurthy et al., 2016; Tan et al., 2019). However, the model performance is greatly influenced by the model resolution. This is on one hand because most of the current global models rely on the detection algorithm to detect the TCs. The coarser the models, the harder the realistic detection of TCs, particularly the total number and intense cases (Oouchi et al., 2006; Camargo, 2013; Murakami et al., 2015). Hence, the higher resolution models toward 25 km generally outperform the lower ones in simulating the global distribution, interannual variation and related precipitation of TCs (Rathmann et al., 2013; Murakami et al., 2015; Roberts et al., 2020; Zhang et al., 2021; Moon et al., 2022). On the other hand, increasing the resolution of CGCM can considerably improve the ENSO simulation such as the power spectra, periodicity, seasonal cycle and amplitude when compared to the same model with a lower resolution, owing to the better representation of mesoscale atmospheric and oceanic processes and thus reduced biases in the air-sea coupling and cold tongue in the tropical Pacific (Guilyardi et al., 2004; Navarra et al., 2008; Hua et al., 2018; Wengel et al., 2021). Hence, using a high-resolution CGCM may have the superiority in simulating the ENSO-WNPTC relationship. Zhang et al. (2016a) did show that the high-resolution GFDL HiFLOR coupled climate model outperforms its low-resolution version in reproducing the observed influences of ENSO on the WNPTCs including the TC track density, genesis and landfall due to better representation of the SST anomalies and the related large-scale circulation anomalies-related to ENSO. However, these results of Zhang et al. (2016a) are drawn based on one single model and may lack of generality. Meanwhile, the underlying mechanism responsible for the improved ENSO-related SST and large-scale circulation anomalies was not analyzed.

Recently, the HighResMIP-PRIMAVERA project released the archive of numerical simulations conducted by a series of CGCMs with the CMIP6-type (~100 km, LR) and higher (~25 km, HR) resolutions in order to explore whether the global modeling and high-resolution add values to our understanding of high-impact weather events (Haarsma et al., 2016; Roberts et al., 2020). A common protocol is provided to restrict the HR model configurations when compared to their LR versions to reflect, to the most extent, the mere impacts of model resolutions. Readers are referred to Haarsma et al. (2016) for details of the experiment setups. Hence, this project provides us the unique opportunity to investigate the ENSO-WNPTC relationship in these state-of-art CGCMs and to estimate possible impacts of model resolution on reproducing the observed ENSO-WNPTC relationship. The rest of the paper is thus organized as follow. Section 2 provides a brief description of data and methods. Simulations of the ENSO-WNPTC in the HighResMIP-PRIMAVERA ensemble with the HR and LR configurations are compared in Section 3. The impacts of model resolution are estimated. Section 4 discusses possible reasons for the different performances between HR and LR configurations. Conclusion and discussion are given in Section 5.

2 Data and methods

The observed TC data during the period 1979-2014 are adopted from the China Meteorological Administration (CMA)'s tropical cyclone database (CMABST; Ying et al., 2014; Lu et al., 2021). The monthly atmospheric variables from the NCEP-DOE Reanalysis 2 (Kanamitsu et al., 2002), the Global Precipitation Climatology Project (GPCP; Adler et al., 2018) and Hadley Centre Sea Ice and Sea Surface Temperature (HadISST; Rayner, 2003) for the same period are also used.

The model outputs of historical runs that consider the historical anthropogenic forcing by six pairs of CGCMs from the HighResMIP-PRIMAVERA project are analyzed. The six coupled models are CMCC-CM2 (Cherchi et al., 2018), CNRM-CM6 (Voldoire et al., 2019), EC-Earth3P (Haarsma et al., 2016), ECMWF-IFS (Roberts et al., 2018), HadGEM3-GC3.1 (Roberts et al., 2019) and MPI-ESM1.2 (Gutjahr et al., 2019). The detailed HR and LR configurations are shown in Table 1. Here, the TC track is detected by the tracking algorithm "TRACK" (Hodges et al., 2017) that it is good at detecting the weak TCs (Roberts et al., 2020). For an easy comparison of anomalous fields between the HR and LR models, the monthly outputs are commonly interpolated into the $1° × 1°$ gird in advance.

In this study, we focus on the WNPTC genesis during July-October (JASO) that counts more than 60% of the annual WNPTCs (Song et al., 2021). The annual-mean TC genesis both in the observations and models are first binned in $5° × 5°$ grid boxes and then applied the nine-point smoothing (Camargo and Sobel, 2005; Zhang et al., 2016a; Kossin et al., 2016; Tan et al., 2019). The Niño3.4 index is the following November-January (NDJ) SST anomalies averaged in the Niño-3.4 region (5°S-5°N, 170°W-120°W). Here, the anomalies are calculated as the deviations from the observed or modeled seasonal cycles. To highlight the impacts of ENSO at the interannual time scale, the 9-year high-pass Fourier filtering is applied to the anomalies before further analyses.

TABLE 1 Brief summary of model configurations. SISL means semi-implicit and semi-Lagrangian. Model detail can be found online (https://www.primavera-h2020.eu/modelling/our-models/).

Institution	CMCC	CERFACS	EC-Earth KNMI; SHMI; BSC; CNR	ECMWF	MOHC; UREAD; NERC	MPI-M
Model Nama	CMCC-CM2	CNRM-CM6	EC-Earth3	ECMWF-IFS	HadGEM3-GC3.1	MPI-ESM-1-2
Resolution names	HR4, VHR4	LR, HR	LR, HR	LR, HR	MM, HM	HR, XR
Model components	CAM4 NEMO CICE	ARPEGE NEMO GELATO	IFS NEMO LIM	IFS cycle43r1 NEMO3.4 LIM2	UM NEMO CICE	ECHAM6.3 MPIOMI1.63 MPIOMI1.63
Atmos dynamical scheme (grid)	Grid point (finite volume, lat-long)	Spectral (linear, reduced Gussian)	Spectral (linear, reduced Gussian)	Spectral (cubic octohedral, reduced Gussian)	Grid point (SISL, lat-long)	Spectral (triangular, Gussian)
Atmos grid name	1×1, 0.25×0.25	Tl127, Tl359	Tl255, Tl511	Tco199, Tco399	N216, N512	T127, T255
Atmos mesh spacing 0N	100, 28	156, 55	78, 39	50, 25	93, 39	104, 52
Atmos mesh spacing 50N	64, 18	142, 50	71, 36	50, 25	60, 25	67, 34
Atmos nominal res (CMIP6)	100, 25	250, 50	100, 50	50, 25	100, 50	100, 50
Atmos model levels (top)	26 (2 hPa)	91 (78.4 km)	91 (0.01 hPa)	91 (0.01 hPa)	85 (85 km)	95 (0.01 hPa)
Ocean grid name	ORCA	ORCA	ORCA	ORCA	ORCA	TP
Ocean nominal res (km)	25, 25	100, 25	100, 25	100, 25	100, 25	40, 40
Ocean levels	50	75	75	75	75	40

Since the anomalies in the WNPTC genesis and SSTs between the El Niño and La Niña developing years are almost the mirror images, the linear regression is adopted in this study for simplicity. And ENSO-driven anomalies (TC genesis density, SST, atmospheric circulation, precipitation, etc.) were calculated by regression on the following NDJ Niño3.4 index so that the main focus of this study is on the impact of model resolution on the simulation of WNPTC activity during the development period of ENSO.

The relative contributions of different physical and thermal processes to the ENSO-related SST anomalies in both HR and LR models are examined through ocean mixed-layer heat budget analysis (An et al., 1999; Jin et al., 2006; Kug et al., 2010). The SST tendency is investigated in a 4-month sliding window from May to October basing on the SST tendency equation:

$$\frac{\partial SST'}{\partial t} = -\bar{u}\frac{\partial T'}{\partial x} - u'\frac{\partial \bar{T}}{\partial x} - u'\frac{\partial T'}{\partial x} - \bar{v}\frac{\partial T'}{\partial y} - v'\frac{\partial \bar{T}}{\partial y} - v'\frac{\partial T'}{\partial y} - \bar{w}\frac{\partial T'}{\partial z}$$
$$- w'\frac{\partial \bar{T}}{\partial z} - w'\frac{\partial T'}{\partial z} + Q + R$$

(1)

where T, u, v, and w represent the ocean temperature, zonal current, meridional current and vertical velocity, respectively. Q is the net surface heat flux anomaly, and R is the residual term caused by entrainment, diffusion, etc. The bar denotes the climatology, and the prime denotes the anomaly. The mean upwelling advection in Eq. 1

can be further decomposed as in many previous studies (Jin and Neelin, 1993; An et al., 1999; Zhang et al., 2007):

$$-\bar{w}\frac{\partial T'}{\partial z} \approx \bar{w}\frac{T'_{sub}}{H} - \bar{w}\frac{T'}{H}$$

(2)

where H is the mixed layer depth (constant 50 m in this study), and the subscript "sub" represents the subsurface layer between 50 and 100 m. Following Ren and Jin (2013) and shown in Eq. 1, the tendency of SST can be determined by six feedbacks and processes after regrouping the terms in the right-hand sides of Eqs 2, 3. They are the mean circulation (MC), the zonal advection feedback (ZA), the Ekman pumping feedback (EK), the thermocline feedback (TH), the nonlinear dynamical heating (NDH), and the thermodynamical damping (TD).

$$\frac{\partial SST'}{\partial t} = MC + ZA + EK + TH + NDH + TD + R$$

(3)

where

$$MC = -\bar{u}\frac{\partial T'}{\partial x} - \bar{v}\frac{\partial T'}{\partial y} - \bar{w}\frac{T'}{H}$$

(4)

$$ZA = -u'\frac{\partial \bar{T}}{\partial x}$$

(5)

$$EK = -v'\frac{\partial \bar{T}}{\partial y} - w'\frac{\partial \bar{T}}{\partial z}$$

(6)
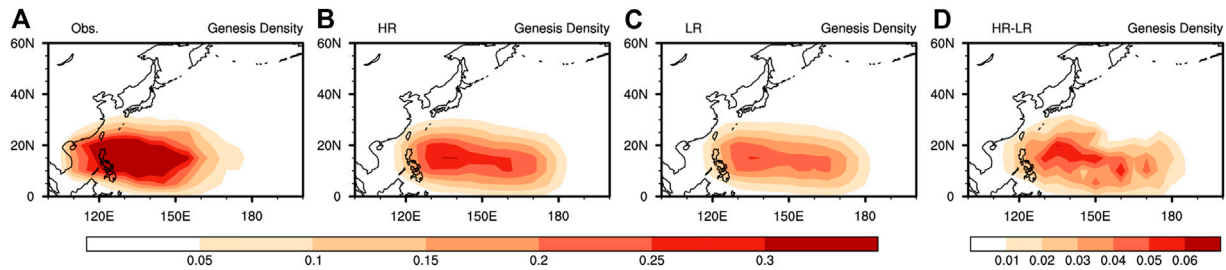
FIGURE 1
Climatological TC genesis densities (units: number year^{-1}, 5° × 5° grid) in the WNP in July-October based on **(A)** the observations and the MMEs of **(B)** HR and **(C)** LR models, and **(D)** the HR-LR differences during 1979−2014.
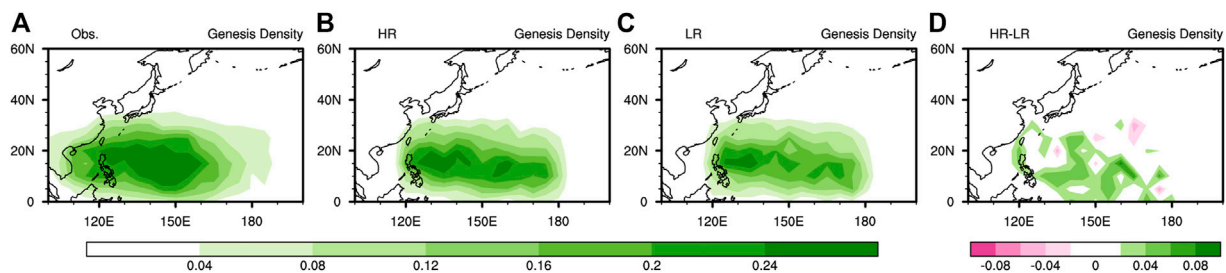
FIGURE 2
The same as in Figure 1, but for the standard deviation of TC genesis densities (units: number year^{-1}, 5° × 5° grid).

$$TH = \bar{w}\frac{T'_{sub}}{H} \tag{7}$$

$$NDH = -u'\frac{\partial T'}{\partial x} - v'\frac{\partial T'}{\partial y} - w'\frac{\partial T'}{\partial z} \tag{8}$$

$$TD = Q \tag{9}$$

$$Q = \frac{Q_{net}}{\rho C_p H} \tag{10}$$

Here, Q_{net} is the net downward radiation flux at the sea surface, that is, the sum of short-wave radiation, long-wave radiation, sensible and latent heat fluxes. ρ and C_p are the density and specific heat capacity of seawater, respectively.

The statistical significance of composite anomalies both in the observations and models are tested by the two tailed t-test. For the differences between the HR and LR configurations of six CGCMs, if the differences have the same signs in over four CGCMs (>67%), they are regarded as significant.

3 Simulated responses of WNPTCs to ENSO in the HR and LR models

The climatological WNPTC genesis densities in JASO during 1979–2014 based on the observations and multi-model ensembles (MMEs) by the HR and LR models are shown in Figure 1. It is clear that both the HR and LR models simulate well the spatial distributions of TC genesis

density in the WNP, but underestimate the frequency (Figures 1A–C). Increasing the model resolution can partly reduce the frequency biases (Figure 1D) as being revealed in the literature (Roberts et al., 2020). The interannual variability of genesis density is also examined in Figure 2. It seems that both the HR and LR models underestimate the interannual variations in the TC genesis (Figures 2A–C), but increasing the resolution can increase the TC variability (Figure 2D). Hence, in general, the HR models outperform the LR ones on reproducing the observed WNPTC mean state and variability (Roberts et al., 2020).

Figure 3 shows the TC genesis anomalies regressed on the Niño3.4 index based on the observations and MMEs. In the TC peak season of El Niño developing years, the observed southeastward shift of WNPTC genesis and the resultant anomalous southeast-northwest oriented dipole pattern can be better simulated by the HR than LR models (Figures 3A–C). The HR models not only simulate the higher anomalous amplitude closer to the observed, but also reproduce better the negative pole in the western WNP (Figures 3B–D). As a result, the pattern correlation coefficient between the observed and simulated TC genesis anomalies is 0.67 in the HR models, larger than that of 0.57 in the LR models (Figures 3A–C). The higher anomalous amplitude in the HR compared to LR models is partly due to the fact that the HR models simulate more frequency occurrence of TCs, which generally leads to the increased amplitude of interannual
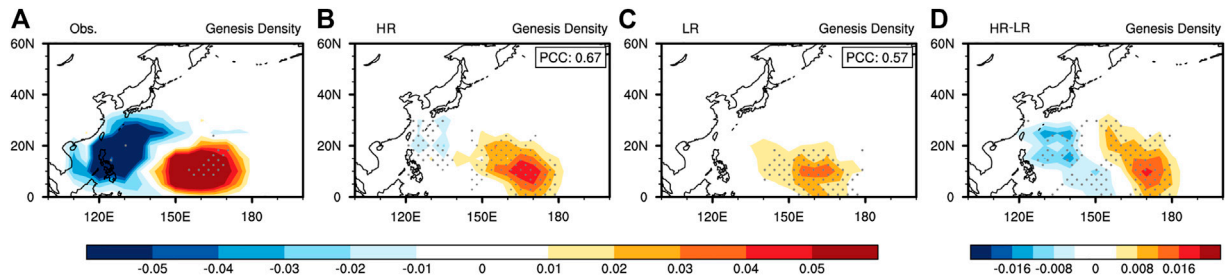
FIGURE 3
The July-October anomalies in TC genesis density (units: number year^{-1}, 5° × 5° grid) regressed on the November–January Niño3.4 index based on (A) the observations and the MMEs of (B) HR and (C) LR models, and (D) HR-LR differences during 1979−2014. The pattern correlation coefficients (PCC) between the observations and HR/LR models are labeled in the top-right corner of the panel. Anomalies significant at the 90% confidence are stippled in (A−C). Differences between the HR and LR models are stippled if 4 out of 6 CGCMs have the same signs in (D).
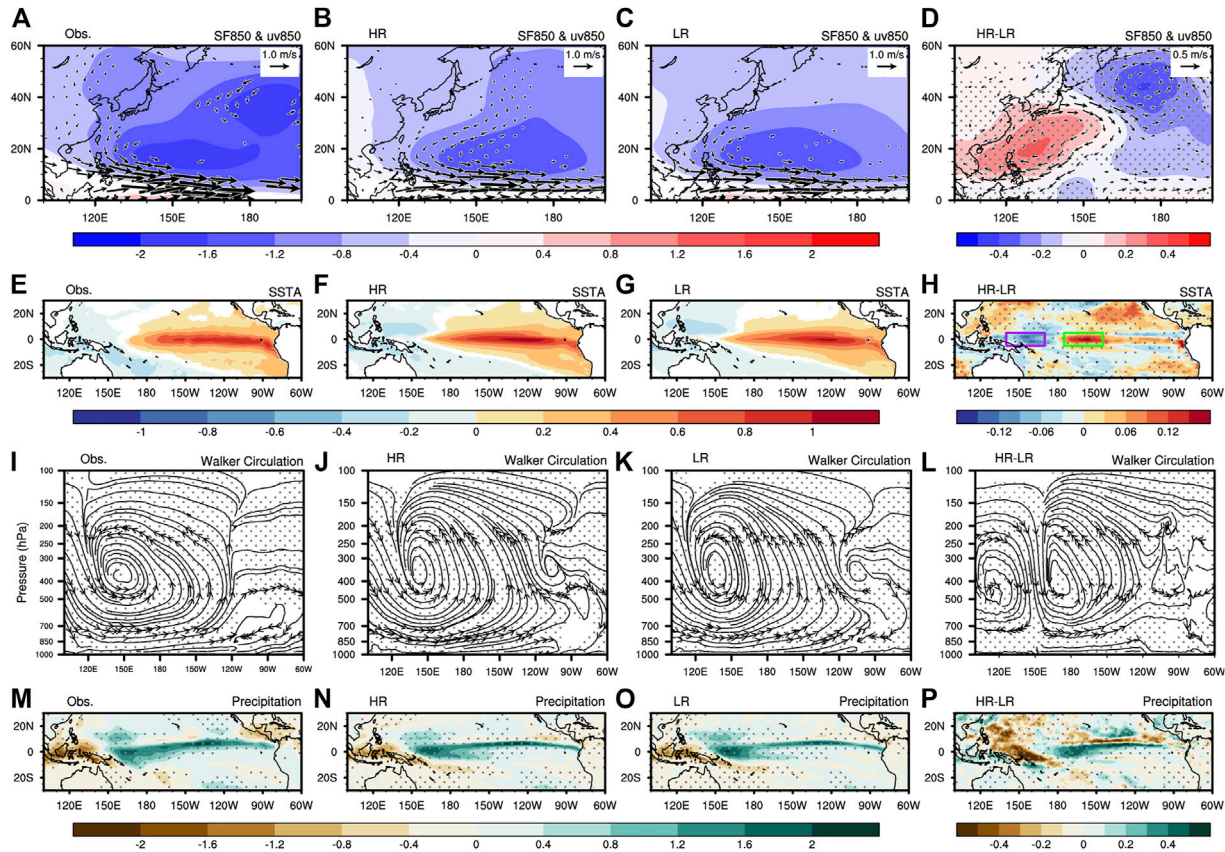
FIGURE 4
The July-October anomalies in (A−C) 850-hPa stream function (shading; units: 10^6 m^2 s^{-1}) and wind (vector; units: m s^{-1}), (E−G) SST (units: °C), (I−K) zonal-vertical circulation averaged between 15°S-15°N with the vertical velocity amplified by a factor of 1000, and (M−O) precipitation (units: mm day^{-1}) in the tropical Pacific regressed on the November-January Niño3.4 index based on (A, E, I, M) the observations, the MMEs of (B, F, J, N) HR and (C, G, K, O) LR models, and (D, H, L, P) the HR-LR differences during 1979−2014. Anomalies significant at the 90% confidence level in wind in (A−C) and SST in (E−G) are shown only, and those in zonal and vertical velocity in (I−K) and precipitation in (M−O) are stippled. Differences between the HR and LR models are stippled if 4 out of 6 CGCMs have the same signs in (D, H, L, P). The purple and green rectangles in (H) denote the regions of Box1 (5°S-5°N, 140°E–170°E) and Box2 (5°S-5°N, 175°W-145°W), respectively.

variability (Figures 2B–D). Further, the El Niño-related teleconnections are slightly different between the HR and LR models; the anomalous cyclone in the WNP, that is, crucial to

convey the El Niño impacts on the WNPTCs extends less westward but further eastward in the HR compared to LR models (Figures 4A–C). Hence, their difference shows an
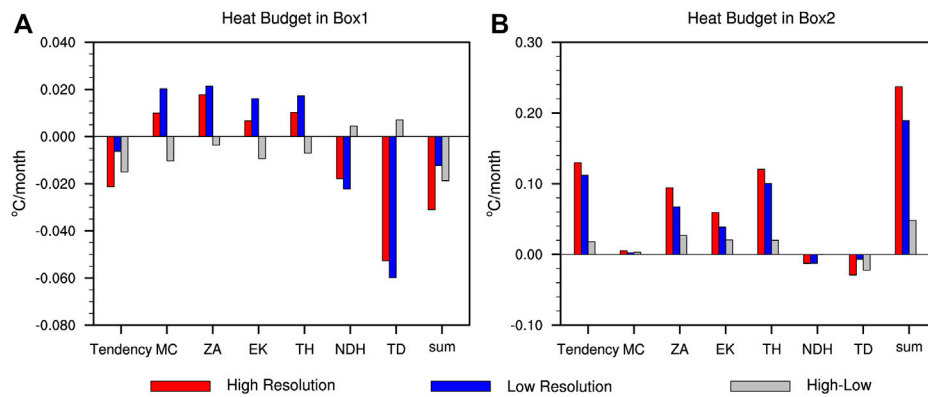
FIGURE 5
The May-October tendencies of SST anomaly in **(A)** Box1 and **(B)** Box2 and the contributions of six processes contributors (units: °C month⁻¹) regressed on the November-January Niño3.4 index based on the MMEs of HR (red bar) and LR (blue bar) models and their difference (grey bar). The total contribution of six processes are summed and presented as the sum term. The six processes are the mean circulation (MC), the zonal advection feedback (ZA), the Ekman pumping feedback (EK), the thermocline feedback (TH), the nonlinear dynamical heating (NDH), and the thermodynamical damping (TD).
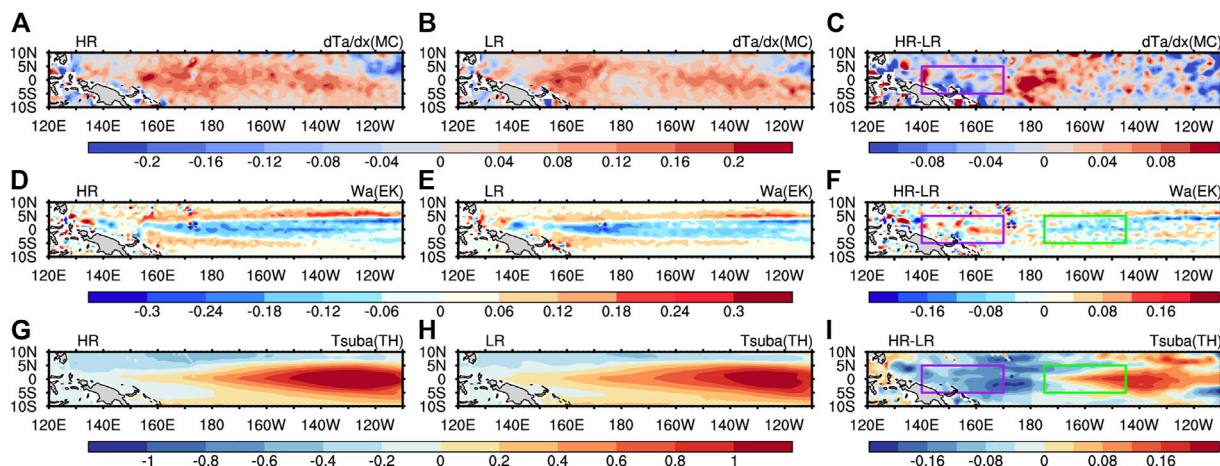
FIGURE 6
The May-October anomalies in **(A, B)** the mixed-layer zonal gradient of SST anomaly (units: 10^{-6} °C m⁻¹) **(D, E)** vertical velocity (units: 10^{-5} m s⁻¹, positive upward), **(G, H)** ocean subsurface temperature averaged between 50−100 m below the surface (units: °C), regressed on November-January Niño3.4 index based on the MMEs of the **(A, D, G)** HR and **(B, E, H)** LR models and **(C, F, I)** their differences.

anomalous anticyclone/cyclone in the western/eastern WNP (Figure 4D), which is conducive to less/more occurrences of TC in the western/eastern WNP in the HR compared to the LR models in the El Niño developing summers (Figure 3D). As a result, the HR models reproduce more realistically the El Niño-related anomalies in the WNPTC genesis (Figures 3A–C). Moreover, the difference of interannual variability is small over the Philippine Sea and mainly in the southwestern WNP (Figure 2D), where interannual variability associated with the monsoon trough is significant (Wu et al., 2012). The subtle difference over the Philippine Sea may means that the better performance of HR in this region (i.e., El Niño suppresses the genesis of TCs, Figure 3) is primarily attributed to the representation of ENSO-related large-scale fields.

The difference in the circulation anomalies in the WNP between the HR and LR models may result from the difference in the simulated El Niño-related SST anomalies in the tropical Pacific (Figures 4A–H). As can be seen in Figures 4E–H, the positive SST anomalies in the HR models extend less westward than those in the LR models, leading to the negative difference between them in the western tropical Pacific referring as Box1 (5°S-5°N, 140°E–170°E). Meanwhile, the positive SST anomalies in the HR models show the higher anomalous amplitudes in the central tropical Pacific referring as Box2 (5°S-5°N, 175°W-145°W). The dipole difference in the SST anomalies between the HR and LR models can lead to the dipole difference in convection and precipitation in the tropical Pacific; less active convection and precipitation in

FIGURE 7
May-October mean state biases in SST (shade; units: °C) and
1000-hPa horizontal wind (vector; units: m s^{-1}) during
1979−2014 between the (A) HR/(B) LR models and observations and
(C) the HR-LR bias differences. Differences in (A−C) are stippled if
4 out of 6 CGCMs have the same signs.

FIGURE 8
Schematic diagram of the HR-LR differences affecting ENSO and
its teleconnection in the WNP.
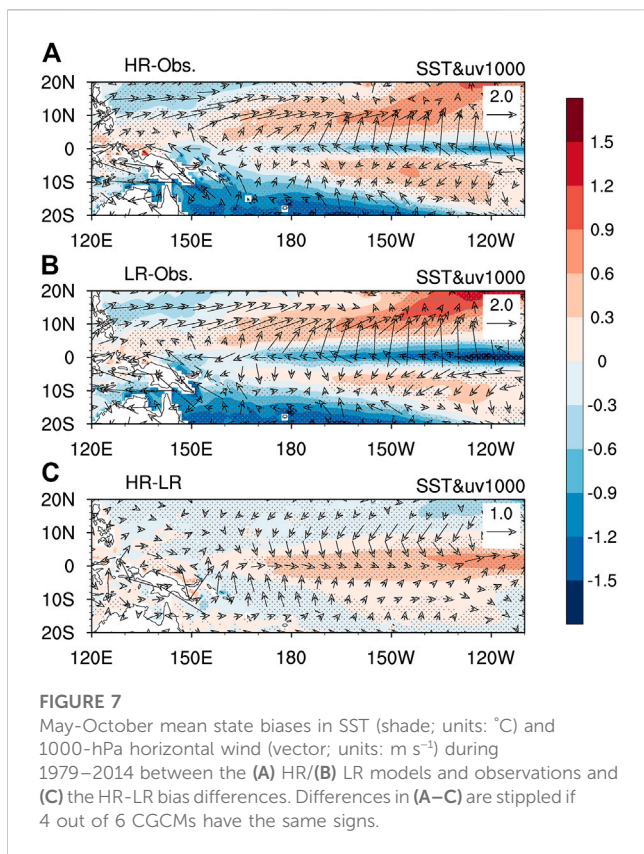
Box1, but more in Box2 (Figures 4I, P). Consequently, the
anticyclonic/cyclonic circulation difference appears in the
western/eastern WNP as the Matsuno-Gill response to the pair
of positive-negative heating difference along the equator
(Matsuno, 1966; Gill, 1980). Hence, less/more TC genesis are
caused in the western/eastern WNP in the HR compared to the
LR models in July-October of the El Niño developing years,
contributing the higher anomalous amplitude in the HR
models (Figure 3D).

4 Simulated SST anomalies related to ENSO in the HR and LR models

As discussed in Section 3, the differences between the responses of
WNPTCs to ENSO in the HR and LR models can be caused by the
differences in the ENSO-related SST anomalies in the tropical Pacific,
particularly in Boxes 1 and 2 Hence, it is interesting to investigate
possible thermal and/or dynamical processes responsible for the
differences. The dipole differences clearly appear in May-August
(MJJA) and enhance thereafter (JASO) in ENSO-related SST and
precipitation anomalies in the western and central tropical Pacific
between the HR and LR models (figures not shown). Thus, only the
May-October averaged SST anomaly tendency and the respective
contributions by the six different processes (Eq. 3) in both the HR
and LR models and their differences are shown in Figure 5.

In Box1 (Figure 5A), it is clear that each process has almost the
same-signed contribution to the SST anomaly tendency in both the
HR and LR models. The MC, ZA, EK and TH enhance the anomalous
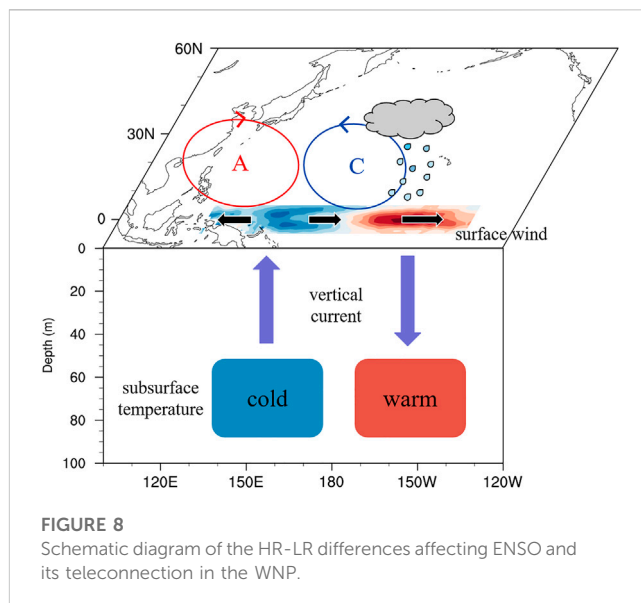
warming, but the NDH and TD suppress it. In the HR models, the
enhancement by the MC, EK and TH are smaller, resulting in the
smaller warming rate in the HR compared to the LR models.
Consequently, the MC, EK, and TH processes all together lower
the JASO SST anomalies in Box1 in the HR models. Further analyses
show that the term $-\bar{u}\frac{\partial T'}{\partial x}$ is responsible for the weaker MC in the HR
models. The zonal gradient of the anomalous SST is positive and
smaller in the HR compared to the LR model due to the less westward
extension of warm SST anomalies related to the El Niño (Figures
6A–C, 4L), causing the smaller MC. For the EK difference, the term of
$-w'\frac{\partial \bar{T}}{\partial z}$ matters most. Although the vertical gradient of climatological
ocean temperature above the thermocline is slightly sharper in the HR
models (figure not shown), the anomalous downward vertical velocity
is smaller due to the weaker surface westerly anomalies (Figure 4L)
and thus the smaller Ekman pumping in Box1 (Figures 6D–F),
leading to the weaker EK in the HR compared to the LR models (Figure 5A).
The weaker westerly anomalies in Box1 also cause the weaker
downwelling Kelvin waves and thus the smaller increase of
subsurface temperature, resluting in the weaker TH in the HR
compared to the LR models (Figures 6G–I).

In Box2 (Figure 5B), the May-October tendency of SST anomaly
is larger in the HR than LR models due to the higher positive
contributions by the ZA, EK and TH. This is not surprising because
in contrast to Box1, the surface westerly anomalies in Box2 are larger
in the HR than LR models (Figure 4L). This leads to the stronger
downwelling Kelvin waves and thus the larger responses of
anomalous eastward zonal current, downward vertical velocity
and increased subsurface temperature, which consequently
enhances the ZA, EK and TH (Figures 6F, I).

As discussed above, the dipole differences of SST anomaly in the
western and central tropical Pacific between the HR and LR models
can be mainly caused by the difference in the overlying surface wind
anomalies. However, the difference in the overlying surface wind
anomalies themselves can be the results of the dipole difference of
SST anomalies, implying the close air-sea interaction in the tropical
Pacific. Hence, it is interesting to reveal how these coupled
differences are initialized. As shown in Figure 7, the cold tongue

FIGURE 9
As in Figures 3B–D, but based on the MME of **(A–C)** the CGCMs with the increased resolution only in the atmospheric components in their HR versions (CMCC-CM2 and MPI-ESM-1-2) and **(D–F)** those with the increased resolution in both the atmospheric and ocean components (CNRM-CM6, EC-Earth3, ECMWF-IFS and HadGEM3-GC3.1).
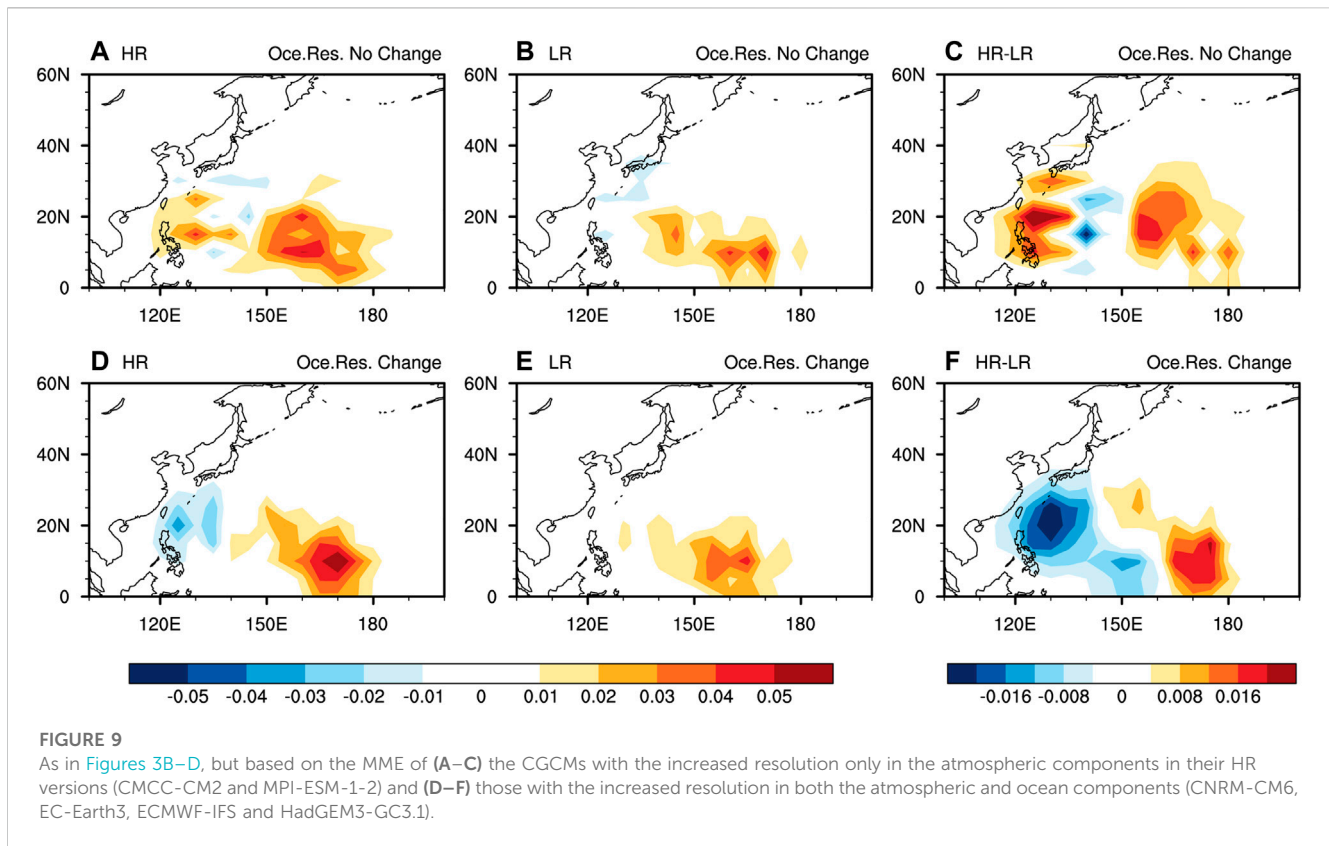
biases in the tropical Pacific appear in both the HR and LR model as being suffered by most state-of-the-art CGCMs (Guilyardi et al., 2009; Zheng et al., 2012; Li and Xie, 2014; Ge and Chen, 2020). However, they are much reduced in the HR compared to LR models (Figure 7C). In other words, the cold tongue in the LR models is too cold and extends too westward (Figures 7A, B). Suppose the tropical Pacific in both the HR and LR models experience the same SST anomalies in the western and central tropical Pacific at the very beginning, it is very likely that the HR models have anomalous convection center more eastward than that in LR models since the convection requires the absolute SST (mean state plus anomaly) higher than a threshold value as suggested by Johnson and Xie. (2010); the colder mean state of LR models thus tends to have the anomalous convection center more westward and closer to the western warm pool to acquire the higher mean-state SST. The eastward shift of the convection in the HR compared to the LR models analogous to Figure 4P causes the differences in the surface wind anomaly analogous to Figure 4L and leads to the dipole difference of the SST anomaly analogous to Figure 4H as analyzed in this section, which again enhances the dipole difference of the precipitation. Hence, the difference in the mean state of tropical Pacific may cause the difference of responses of ENSO center, its teleconnection and climate impacts.

5 Conclusion and discussion

The ENSO is one of the major drivers of interannual variations in the WNPTC activity. Hence, accurate simulation and prediction of the ENSO impacts are vital for proper adaptation planning and decision-making to mitigate potential damages caused by the TCs. In this study, basing on the HighResMIP-PRIMAVERA project, we have compared the performance of six pairs of HR and LR models on reproducing the observed ENSO impacts on the WNPTCs. Results show that the HR models outperform the LR ones in reproducing the increased TC genesis over the southeastern WNP but the decreased over the northwestern WNP in the developing years of El Niño. The better performance of HR is on one hand due to the generally increased frequency and variability of the TCs in the HR models. On the other hand, the ENSO teleconnection to the WNP shows a dipole circulation difference in the lower troposphere with the cyclonic circulation difference in the southeastern WNP but the anticyclonic in the northwestern WNP, which enhances the dipole TC genesis anomalies in the HR compared to LR models. The dipole circulation difference in the WNP can stem from the dipole difference in the ENSO-related SST anomalies in the tropical Pacific between the HR and LR models. The El Niño-related positive SST anomalies are lower in the western tropical Pacific, but higher in the central tropical Pacific in the HR compared to the LR models. This can lead to the pair of negative-positive difference in convection and diabatic heating along the equator and thus the pair of anticyclone-cyclone circulation difference in the WNP as the Matsuno-Gill response. Further analyses show that the pair of negative-positive difference in the El Niño-related SST anomalies can be mainly caused by the difference in the convection-related surface zonal wind anomalies via the Ekman, zonal advection and thermocline feedbacks, indicating the close air-sea coupling in the tropical Pacific (Figure 8).

The possible trigger of these coupled differences in the surface wind, convection and SST anomalies may be the smaller cold tongue biases in the HR compared to the LR models. The higher mean-state SSTs in the tropical Pacific enable the El Niño-related convection shift more eastward in the HR than LR models, resulting in the pair of negative-positive convection difference and the consequent surface wind and SST differences, which can reversely enhance the initial convection difference. The equatorial cold tongue bias commonly exits in many CGCMs and is considered to be closely related to the bias in the Intertropical Convergence Zone and the misrepresentation of mesoscale atmospheric and oceanic processes (Li and Xie, 2014; Xiang et al., 2017; Bayr et al., 2018; Tian and Dong, 2020; Zhou et al., 2020; Si et al., 2021). This study shows that increasing the CGCM resolution can reduce the cold tongue bias and improve the simulation of the observed ENSO-WNPTC teleconnection. However, it is difficult to quantitatively attribute the improvement to the increased atmospheric or oceanic components since the higher resolution in either atmospheric or oceanic models could improve ENSO and its teleconnection simulations (Roberts et al., 2004; Navarra et al., 2008; Dawson et al., 2013; Small et al., 2014; Hua et al., 2018). Here, four of six HR CGCMs have the increased resolutions in both the atmospheric and oceanic components and the rest two only increase the atmospheric component (Table 1). We have compared the performance of the two groups. It is found that the group with the increased atmospheric and oceanic resolutions have better improvement than the group with the increased atmospheric resolution only when compared to their LR versions (Figures 3, 9). However, the results should be interpreted with cautions due to the small number of models in each group and lack of statistical significance.

Previous studies have shown that locations of the maximum SST anomalies related to ENSO can modulate the ENSO impacts on the WNP TC activity (Chen and Tam, 2010; Zhang et al., 2012; Patricola et al., 2016; Zhao and Wang, 2018). Although both the eastern Pacific El Niño (EPE) and central Pacific El Niño (CPE) can cause the dipole anomalies in the WNP TC genesis, the horizontal location of the dipole related to the CPE is more westward compared to the EPE due to the more westward anomalous warming of CPE (Kim et al., 2011; Song et al., 2021). However, the models in HighResMIP-PRIMAVERA project have poor performance in the diversity of El Niño events, there are few differences in the simulation of WNPTCs activity between different El Niño events. Investigating why the models cannot distinguish the two types of ENSO become an intriguing question. In addition, the ENSO can prolong its impacts on the climate in the Indo-Pacific sector in its decaying summer via the Indo-western Pacific Ocean capacitor (IPOC) effect (Xie et al., 2009; 2016; Du et al., 2011; Zhan et al., 2011; Takaya et al., 2021). The observed anomalous warming in the northern Indian Ocean and WNP, the anomalous anticyclone and thus suppressed TC genesis in the WNP are well simulated by both the HR and LR models during the decaying summer of El Niño (Xie et al., 2009; 2016; Du et al., 2011). However, the anomalous amplitudes of both anticyclone and TC genesis density are higher and closer to the observed in the HR compared to the LR models (figures not shown). This is probably because the anomalous warming in the southeastern tropical Indian Ocean is much higher in the HR than LR models since the anomalous warming there can lead to the anomalous anticyclone and less TC genesis in the WNP (Zhan et al., 2011; Tao et al., 2017).

The CGCM biases not only influence the simulation of ENSO and its teleconnection under the present climate, but also impact the future projection of ENSO. Tang et al. (2021) corrected several common biases in the tropical oceans in the CGCMs participating the phase 5 of coupled model intercomparison project (CMIP5), and found no significant changes in frequency of the extreme El Niño under the RCP8.5 scenario, which is contrasted to Cai et al. (2017) who showed a significant increase. This indicates that when interpreting the future projection of ENSO and its climate effects by using the CGCMs, possible influences from the model biases should be considered. In short, continuous efforts are needed to understand the origins of and to reduce the model biases for better simulation, prediction and projection of our climate systems.

Data availability statement

The original contributions presented in the study are included in the article/Supplementary Material, further inquiries can be directed to the corresponding author.

Author contributions

All authors contributed to the study conception and design. Material preparation, data collection and analysis were performed by JL, CY, and J-JL. The first draft of the manuscript was written by JL, CY, and J-JL, and all authors commented on previous versions of the manuscript. All authors read and approved the final manuscript. All authors listed have made a substantial, direct, and intellectual contribution to the work and approved it for publication.

Conflict of interest

The authors declare that the research was conducted in the absence of any commercial or financial relationships that could be construed as a potential conflict of interest.

Publisher's note

All claims expressed in this article are solely those of the authors and do not necessarily represent those of their affiliated organizations, or those of the publisher, the editors and the reviewers. Any product that may be evaluated in this article, or claim that may be made by its manufacturer, is not guaranteed or endorsed by the publisher.

References

Adler, R. F., Sapiano, M. R. P., Huffman, G. J., Wang, J. J., Gu, G., Bolvin, D., et al. (2018). The Global Precipitation Climatology Project (GPCP) monthly analysis (new version 2.3) and a review of 2017 global precipitation. *Atmos* 9 (4), 138–151. doi:10.3390/atmos9040138

An, S., Jin, F. F., and Kang, I. S. (1999). The role of zonal advection feedback in phase transition and growth of ENSO in the Cane-Zebiak model. *J. Meteorol. Soc. Jpn.* 77 (6), 1151–1160. doi:10.2151/jmsj1965.77.6_1151

Bayr, T., Latif, M., Dommenget, D., Wengel, C., Harla, J., and Park, W. (2018). Mean-state dependence of ENSO atmospheric feedbacks in climate models. *Clim. Dyn.* 50 (9), 3171–3194. doi:10.1007/s00382-017-3799-2

Bell, R., Hodges, K., Vidale, P. L., Strachan, J., and Roberts, M. (2014). Simulation of the global ENSO-tropical cyclone teleconnection by a high-resolution coupled general circulation model. *J. Clim.* 27 (17), 6404–6422. doi:10.1175/jcli-d-13-00559.1

Cai, W., Wang, G., Santoso, A., Lin, X., and Wu, L. (2017). Definition of extreme El Niño and its impact on projected increase in extreme El Niño frequency. *Geophys. Res. Lett.* 44 (21), 11184–11190. doi:10.1002/2017GL075635

Camargo, S. J. (2013). Global and regional aspects of tropical cyclone activity in the CMIP5 models. *J. Clim.* 26 (24), 9880–9902. doi:10.1175/jcli-d-12-00549.1

Camargo, S. J., and Sobel, A. H. (2005). Western North Pacific tropical cyclone intensity and ENSO. *J. Clim.* 18 (15), 2996–3006. doi:10.1175/JCLI3457.1

Chan, J. C. L. (2000). Tropical cyclone activity over the Western North pacific associated with El Niño and La Niña events. *J. Clim.* 13 (16), 2960–2972. doi:10.1175/1520-0442(2000)013<2960:TCAOTW>2.0.CO;2

Chen, G., and Tam, C. Y. (2010). Different impacts of two kinds of Pacific Ocean warming on tropical cyclone frequency over the Western North Pacific. *Geophys. Res. Lett.* 37, L01803. doi:10.1029/2009GL041708

Cherchi, A., Fogli, P. G., Lovato, T., Peano, D., Iovino, D., Gualdi, S., et al. (2018). Global mean climate and main patterns of variability in the CMCC-CM2 Coupled Model. *J. Adv. Model. Earth Syst.* 11 (1), 2018MS001369–209. doi:10.1029/2018ms001369

Chih, C. H., and Wu, C. C. (2020). Exploratory analysis of upper-ocean heat content and sea surface temperature underlying tropical cyclone rapid intensification in the Western North Pacific. *J. Clim.* 33 (3), 1031–1050. doi:10.1175/jcli-d-19-0305.1

Dawson, A., Matthews, A. J., Stevens, D. P., Roberts, M. J., and Vidale, P. L. (2013). Importance of oceanic resolution and mean state on the extra-tropical response to El Niño in a matrix of coupled models. *Clim. Dyn.* 41 (5-6), 1439–1452. doi:10.1007/s00382-012-1518-6

Du, Y., Yang, L., and Xie, S. P. (2011). Tropical Indian Ocean influence on Northwest Pacific tropical cyclones in summer following strong El Niño. *J. Clim.* 24, 315–322. doi:10.1175/2010JCLI3890.1

Elsberry, R. L. (2004). "Monsoon-related tropical cyclones in East Asia," in *East asian monsoon*. Editor C. P. Chang (Singapore: World Scientific Press), 463–498.

Emanuel, K. A. (2005). *Divine wind*. London: Oxford University Press.

Ge, Z., and Chen, L. (2020). Preliminary analysis of the zonal distribution of ENSO-related SSTA in three CMIP5 coupled models. *Atmos. Ocean. Sci. Lett.* 13, 443–451. doi:10.1080/16742834.2020.1775475

Gill, A. E. (1980). Some simple solutions for heat-induced tropical circulation. *Q. J. R. Meteorol. Soc.* 106 (449), 447–462. doi:10.1002/qj.49710644905

Gong, Z., Li, B., Tang, J., Yang, Y., Li, Z., Liu, M., et al. (2022). Gut microbiota links with cognitive impairment in amyotrophic lateral sclerosis: A multi-omics study. *Front. Earth. Sci.* 10, 1–13. doi:10.7555/JBR.36.20220198

Gray, W. M. (1979). "Hurricanes: Their formation, structure and likely role in the tropical circulation," in *Meteorology over the tropical oceans*. Editor D. B. Shaw (London: Royal Meteorological Society Press), 155–218.

Guilyardi, E. A., Wittenberg, A., Fedorov, A., Collins, M., Wang, C., Capotondi, A., et al. (2009). Understanding El Niño in ocean-atmosphere general circulation models: Progress and challenges. *Bull. Am. Mete. Soc.* 90 (3), 325–340. doi:10.1175/2008bams2387.1

Guilyardi, E., Gualdi, S., Slingo, J., Navarra, A., Delecluse, P., Cole, J., et al. (2004). Representing El Niño in coupled ocean-atmosphere GCMs: The dominant role of the atmospheric component. *J. Clim.* 17 (24), 4623–4629. doi:10.1175/jcli-3260.1

Gutjahr, O., Putrasahan, D., Lohmann, K., Jungclaus, J. H., von Storch, J. S., Brüggemann, N., et al. (2019). Max planck institute Earth system model (MPI-ESM1.2) for the high-resolution model intercomparison project (HighResMIP). *Geosci. Model. Dev.* 12 (7), 3241–3281. doi:10.5194/gmd-12-3241-2019

Haarsma, R. J., Roberts, M. J., Vidale, P. L., Senior, C. A., Bellucci, A., Bao, Q., et al. (2016). High resolution model intercomparison project (HighResMIP v1.0) for CMIP6. *Geosci. Model. Dev.* 9 (11), 4185–4208. doi:10.5194/gmd-9-4185-2016

Hodges, K., Cobb, A., and Vidale, P. L. (2017). How well are tropical cyclones represented in reanalysis datasets? *J. Clim.* 30 (14), 5243–5264. doi:10.1175/JCLI-D-16-0557.1

Hua, L., Chen, L., Rong, X., Su, J., Wang, L., Li, T., et al. (2018). Impact of atmospheric model resolution on simulation of ENSO feedback processes: A coupled model study. *Clim. Dyn.* 51 (7-8), 3077–3092. doi:10.1007/s00382-017-4066-2

Iizuka, S., and Matsuura, T. (2007). ENSO and Western North Pacific tropical cyclone activity simulated in a CGCM. *Clim. Dyn.* 30 (7-8), 815–830. doi:10.1007/s00382-007-0326-x

Jia, L. L. (2007). The double-ITCZ problem in IPCC AR4 coupled GCMs: Ocean-atmosphere feedback analysis. *J. Clim.* 20 (18), 4497–4525. doi:10.1175/jcli4272.1

Jin, F. F., Kim, S. T., and Bejarano, L. (2006). A coupled-stability index for ENSO. *Geophys. Res. Lett.* 33 (23), L23708. doi:10.1029/2006gl027221

Jin, F. F., and Neelin, J. D. (1993). Modes of interannual tropical ocean-atmosphere interaction-A unified view. Part I: Numerical results. *J. Atmos. Sci.* 50 (21), 3477–3503. doi:10.1175/1520-0469(1993)050<3477:MOITOI>2.0.CO;2

Johnson, N. C., and Xie, S. P. (2010). Changes in the sea surface temperature threshold for tropical convection. *Nat. Geosci.* 3 (12), 842–845. doi:10.1038/ngeo1008

Kanamitsu, M., Wesley, E., Woollen, J., Yang, S. K., Hnilo, J. J., Fiorino, M., et al. (2002). NCEP-DOE AMIP-II reanalysis (R-2). *Bull. Am. Mete. Soc.* 83 (11), 1631–1644. doi:10.1175/bams-83-11-1631

Kim, H. M., Webster, P. J., and Curry, J. A. (2011). Modulation of North Pacific tropical cyclone activity by three phases of ENSO. *J. Clim.* 24, 1839–1849. doi:10.1175/2010JCLI3939.1

Kossin, J. P., Emanuel, K. A., and Camargo, S. J. (2016). Past and projected changes in Western North Pacific tropical cyclone exposure. *J. Clim.* 29 (16), 5725–5739. doi:10.1175/jcli-d-16-0076.1

Krishnamurthy, L., Vecchi, G. A., Msadek, R., Murakami, H., Wittenberg, A., and Zeng, F. (2016). Impact of strong ENSO on regional tropical cyclone activity in a high-resolution climate model in the North Pacific and North Atlantic Oceans. *J. Clim.* 29 (7), 2375–2394. doi:10.1175/jcli-d-15-0468.1

Kug, J. S., Choi, J., An, S., Jin, F. F., and Wittenberg, A. T. (2010). Warm pool and cold tongue El Niño events as simulated by the GFDL 2.1 Coupled GCM. *J. Clim.* 23 (5), 1226–1239. doi:10.1175/2009jcli3293.1

Li, G., and Xie, S. P. (2014). Tropical biases in CMIP5 multimodel ensemble: The excessive equatorial Pacific cold tongue and double ITCZ problems. *J. Clim.* 27 (4), 1765–1780. doi:10.1175/jcli-d-13-00337.1

Lu, X., Yu, H., Ying, M., Zhao, B., Zhang, S., Lin, L., et al. (2021). Western North pacific tropical cyclone database created by the China meteorological administration. *Adv. Atmos. Sci.* 38 (4), 690–699. doi:10.1007/s00376-020-0211-7

Matsuno, T. (1966). Quasi-Geostrophic motions in the equatorial area. *J. Meteorol. Soc. Jpn.* 44 (1), 25–43. doi:10.2151/jmsj1965.44.1_25

Moon, Y., Kim, D., Wing, A. A., Camargo, S. J., Zhao, M., Leung, L. R., et al. (2022). An evaluation of tropical cyclone rainfall structures in the HighResMIP simulations against satellite observations. *J. Clim.* 35 (22), 7315–7338. doi:10.1175/JCLI-D-21-0564.1

Murakami, H., Vecchi, G. A., Underwood, S., Delworth, T. L., Wittenberg, A. T., Anderson, W. G., et al. (2015). Simulation and prediction of category 4 and 5 hurricanes in the high-resolution GFDL HiFLOR coupled climate model. *J. Clim.* 28 (23), 9058–9079. doi:10.1175/jcli-d-15-0216.1

Murakami, H., Wang, B., and Kitoh, A. (2011). Future change of Western North pacific typhoons: Projections by a 20-km-mesh global atmospheric model. *J. Clim.* 24 (4), 1154–1169. doi:10.1175/2010jcli3723.1

Navarra, A., Gualdi, S., Masina, S., Behera, S., Luo, J. J., Masson, S., et al. (2008). Atmospheric horizontal resolution affects tropical climate variability in coupled models. *J. Clim.* 21 (4), 730–750. doi:10.1175/2007jcli1406.1

Oouchi, K., Yoshimura, J., Yoshimura, H., Mizuta, R., Kusunoki, S., and Noda, A. (2006). Tropical cyclone climatology in a global-warming climate as simulated in a

20 km-mesh Global Atmospheric Model: Frequency and wind intensity analyses. *J. Meteorol. Soc. Jpn.* 84 (2), 259–276. doi:10.2151/jmsj.84.259

Patricola, C. M., Chang, P., and Saravanan, R. (2016). Degree of simulated suppression of Atlantic tropical cyclones modulated by flavour of El Niño. *Nat. Geosci.* 9, 155–160. doi:10.1038/ngeo2624

Peduzzi, P., Chatenoux, B., Dao, H., Bono, A., and Herold, C. (2012). Global trends in tropical cyclone risk. *Nat. Clim. Change* 2 (4), 289–294. doi:10.1038/nclimate1410

Rathmann, N. M., Yang, S., and Kaas, E. (2013). Tropical cyclones in enhanced resolution CMIP5 experiments. *Clim. Dyn.* 42 (3-4), 665–681. doi:10.1007/s00382-013-1818-5

Rayner, N. A. (2003). Global analyses of sea surface temperature, sea ice, and night marine air temperature since the late nineteenth century. *J. Geophys. Res.* 108 (14), 4407. doi:10.1029/2002jd002670

Ren, H. L., and Jin, F. F. (2013). Recharge oscillator mechanisms in two types of ENSO. *J. Clim.* 26 (17), 6506–6523. doi:10.1175/jcli-d-12-00601.1

Ritchie, E. A., and Holland, G. J. (1999). Large-scale patterns associated with tropical cyclogenesis in the western pacific. *Mon. Weather. Rev.* 127 (9), 2027–2043. doi:10.1175/1520-0493(1999)127<2027:lspawt>2.0.co;2

Roberts, C. D., Senan, R., Molteni, F., Boussetta, S., Mayer, M., and Keeley, S. P. E. (2018). Climate model configurations of the ECMWF integrated forecasting system (ECMWF-IFS cycle 43r1) for HighResMIP. *Geosci. Model. Dev.* 11 (9), 3681–3712. doi:10.5194/gmd-11-3681-2018

Roberts, M. J., Baker, A., Blockley, E. W., Calvert, D., Coward, A., Hewitt, H. T., et al. (2019). Description of the resolution hierarchy of the global coupled HadGEM3-GC3.1 model as used in CMIP6 HighResMIP experiments. *Geosci. Model. Dev.* 12 (12), 4999–5028. doi:10.5194/gmd-12-4999-2019

Roberts, M. J., Banks, H., Gedney, N., Gregory, J., Hill, R., Mullerworth, S., et al. (2004). Impact of an eddy-permitting ocean resolution on control and climate change simulations with a global coupled GCM. *J. Clim.* 17 (1), 3–20. doi:10.1175/1520-0442(2004)017<0003:IOAEOR>2.0.CO;2

Roberts, M. J., Camp, J., Seddon, J., Vidale, P. L., Hodges, K., Vanniere, B., et al. (2020). Impact of model resolution on tropical cyclone simulation using the HighResMIP-PRIMAVERA multimodel ensemble. *J. Clim.* 33 (7), 2557–2583. doi:10.1175/jcli-d-19-0639.1

Shay, L. K., Goni, G. J., and Black, P. G. (2000). Effects of a warm oceanic feature on Hurricane Opal. *Mon. Weather Rev.* 128 (5), 1366–1383. doi:10.1175/1520-0493(2000)128<1366:EOAWOF>2.0.CO;2

Si, W., Liu, H., Zhang, X., and Zhang, M. (2021). Double intertropical convergence zones in coupled ocean-atmosphere models: Progress in CMIP6. *Geophys. Res. Lett.* 48, e2021GL094779. doi:10.1029/2021GL094779

Small, R. J., Bacmeister, J., Bailey, D., Baker, A., Bishop, S., Bryan, F., et al. (2014). A new synoptic scale resolving global climate simulation using the Community Earth System. Model. *J. Adv. Model. Earth Syst.* 6 (4), 1065–1094. doi:10.1002/2014ms000363

Song, J., Klotzbach, P. J., and Duan, Y. (2021). Statistical linkage between coastal El Niño-Southern Oscillation and tropical cyclone formation over the Western North Pacific. *Atmos. Sci. Lett.* 23 (2), 1071. doi:10.1002/asl.1071

Takaya, Y., Kosaka, Y., Watanabe, M., and Maeda, S. (2021). Skilful predictions of the Asian summer monsoon one year ahead. *Nat. Commun.* 12, 2094. doi:10.1038/s41467-021-22299-6

Tan, K., Huang, P., Liu, F., Murakami, H., and Hsu, P. C. (2019). Simulated ENSO's impact on tropical cyclone Genesis over the Western North Pacific in CMIP5 models and its changes under global warming. *Int. J. Climatol.* 39 (8), 3668–3678. doi:10.1002/joc.6031

Tang, T., Luo, J. J., Peng, K., Qi, L., and Tang, S. (2021). Over-projected Pacific warming and extreme El Niño frequency due to CMIP5 common biases. *Natl. Sci. Rev.* 8 (10), nwab056. doi:10.1093/nsr/nwab056

Tao, L., Li, T., Ke, Y. H., and Zhao, J. W. (2017). Causes of interannual and interdecadal variations of the summertime Pacific-Japan-like pattern over East Asia. *J. Clim.* 30 (22), 8845–8864. doi:10.1175/JCLI-D-15-0817.1

Tian, B., and Dong, X. (2020). The double-ITCZ bias in CMIP3, CMIP5 and CMIP6 models based on annual mean precipitation. *Geophys. Res. Lett.* 47, e2020GL087232. doi:10.1029/2020GL087232

Vecchi, G. A., Delworth, T. L., Gudgel, R., Kapnick, S., Rosati, A., Wittenberg, A. T., et al. (2014). On the seasonal forecasting of regional tropical cyclone activity. *J. Clim.* 27 (21), 7994–8016. doi:10.1175/jcli-d-14-00158.1

Voldoire, A., Saint, M. D., Sénési, S., Decharme, B., Alias, A., Chevallier, M., et al. (2019). Evaluation of CMIP6 DECK experiments with CNRM-CM6-1. *J. Adv. Model. Earth. Syst.* 11 (7), 2177–2213. doi:10.1029/2019MS001683

Wang, B., and Chan, J. C. L. (2002). How strong ENSO events affect tropical storm activity over the Western North Pacific. *J. Clim.* 15 (13), 1643–1658. doi:10.1175/1520-0442(2002)015<1643:HSEEAT>2.0.CO;2

Wengel, C., Lee, S. S., Stuecker, M. F., Timmermann, A., Chu, J. E., and Schloesser, F. (2021). Future high-resolution El niño/southern oscillation dynamics. *Nat. Clim. Change* 11, 758–765. doi:10.1038/s41558-021-01132-4

Wu, G., and Lau, N. C. (1992). AGCM simulation of the relationship between tropical-storm formation and ENSO. *Mon. Weather. Rev.* 120 (6), 958–977. doi:10.1175/1520-0493(1992)120,0958:AGSOTR.2.0.CO;2

Wu, L., Wen, Z., Huang, R., and Wu, R. (2012). Possible linkage between the monsoon trough variability and the tropical cyclone activity over the Western North Pacific. *Mon. Weather Rev.* 140, 140–150. doi:10.1175/MWR-D-11-00078.1

Xiang, B., Zhao, M., Held, I. M., and Golaz, J. C. (2017). Predicting the severity of spurious "double ITCZ" problem in CMIP5 coupled models from AMIP simulations. *Geophys. Res. Lett.* 44, 1520–1527. doi:10.1002/2016GL071992

Xie, S. P., Hu, K., Hafner, J., Tokinaga, H., Du, Y., Huang, G., et al. (2009). Indian Ocean capacitor effect on Indo-Western Pacific climate during the summer following El Niño. *J. Clim.* 22, 730–747. doi:10.1175/2008JCLI2544.1

Xie, S. P., Kosaka, Y., Du, Y., Hu, K., Chowdary, J., and Huang, G. (2016). Indo-Western Pacific Ocean capacitor and coherent climate anomalies in post-ENSO summer: A review. *Adv. Atmos. Sci.* 33, 411–432. doi:10.1007/s00376-015-5192-6

Ying, M., Zhang, W., Yu, H., Lu, X., Feng, J., Fan, Y., et al. (2014). An overview of the China Meteorological Administration tropical cyclone database. *J. Atmos. Ocean. Technol.* 31 (2), 287–301. doi:10.1175/jtech-d-12-00119.1

Zhan, R. F., Wang, Y. Q., and Wu, C. C. (2011). Impact of ssta in the East Indian ocean on the frequency of northwest pacific tropical cyclones: A regional atmospheric model study. *J. Clim.* 24, 6227–6242. doi:10.1175/JCLI-D-10-05014.1

Zhang, Q., Kumar, A., Xue, Y., Wang, W., and Jin, F. F. (2007). Analysis of the ENSO cycle in the NCEP coupled forecast model. *J. Clim.* 20 (7), 1265–1284. doi:10.1175/jcli4062.1

Zhang, Q., Wu, L., and Liu, Q. (2009). Tropical cyclone damages in China: 1983-2006. *Bull. Am. Mete. Soc.* 90 (4), 489–496. doi:10.1175/2008BAMS2631.1

Zhang, W., Graf, H. F., Leung, Y., and Herzog, M. (2012). Different El Niño types and tropical cyclone landfall in East Asia. *J. Clim.* 25, 6510–6523. doi:10.1175/JCLI-D-11-00488.1

Zhang, W., Vecchi, G. A., Murakami, H., Delworth, T., Wittenberg, A. T., Rosati, A., et al. (2016a). Improved simulation of tropical cyclone responses to ENSO in the Western North Pacific in the High-Resolution GFDL HiFLOR coupled climate model. *J. Clim.* 29 (4), 1391–1415. doi:10.1175/jcli-d-15-0475.1

Zhang, W., Villarini, G., Scoccimarro, E., Roberts, M., Vidale, P. L., Vanniere, B., et al. (2021). Tropical cyclone precipitation in the HighResMIP atmosphere-only experiments of the PRIMAVERA project. *Clim. Dyn.* 57 (1-2), 253–273. doi:10.1007/s00382-021-05707-x

Zhang, W. Z., Lin, S., and Jiang, X. M. (2016b). "Influence of tropical cyclones in the Western North Pacific," in *Recent developments in tropical cyclone dynamics, prediction, and detection*. Editor R. L. Anthon (London: IntechOpen Press).

Zhao, H., and Wang, C. (2018). On the relationship between ENSO and tropical cyclones in the Western North Pacific during the boreal summer. *Clim. Dyn.* 52 (1-2), 275–288. doi:10.1007/s00382-018-4136-0

Zhao, X. (2019). Research advances on spatial and temporal characteristics of tropical cyclones landfalling in China in the past 50 years and their impacts on agriculture. *J. Mar. Meteor.* 39 (4), 1–11. doi:10.19513/j.cnki.issn2096-3599.2019.04.001

Zheng, Y., Lin, J. L., and Shinoda, T. (2012). The equatorial Pacific cold tongue simulated by IPCC AR4 coupled GCMs: Upper ocean heat budget and feedback analysis. *J. Geophys. Res.* 117 (C5), C05024. doi:10.1029/2011jc007746

Zhou, S., Huang, G., and Huang, P. (2020). Excessive ITCZ but negative SST biases in the tropical Pacific simulated by CMIP5/6 models: The role of the meridional pattern of SST bias. *J. Clim.* 33 (12), 5305–5316. doi:10.1175/JCLI-D-19-0922.1